conference papers

Measurement of self-diffusion constant with two-dimensional X-ray photon correlation spectroscopy

Aymeric Robert‡

ESRF, Avenue Jules Horowitz, BP 220, F-38043 Grenoble Cedex, France, and SLAC, Stanford University, 2575 Sand Hill Road, Menlo Park, CA 94025, USA. Correspondence e-mail: aymeric@slac.stanford.edu

The X-ray photon correlation spectroscopy technique probes the slow dynamics of disordered materials, overcoming the limitations of using photon correlation spectroscopy with coherent visible light. It extends the accessible range of the modulus of the scattering vector to short wavelength density fluctuations and is not sensitive to multiple scattering. We measure here experimentally the short-time self-diffusion coefficient D_S of a charge-stabilized colloidal dispersion. It is in contradiction with theoretical models including many-body hydrodynamic interactions.

1. Introduction

One of the outstanding properties of third-generation synchrotron-radiation sources is their ability to produce coherent X-ray beams several orders of magnitude more intense than previously available. The access to coherent X-rays opens up a variety of possibilities for new techniques such as X-ray photon correlation spectroscopy (XPCS) [Grübel & Zontone (2004) and references therein]. Complex relaxations in disordered systems have been studied successfully using both visible coherent light and neutron scattering techniques.

Photon correlation spectroscopy techniques with coherent visible light (also called dynamic light scattering, DLS) can cover the low-frequency dynamics ($\omega < 10^7$ Hz) but probe only the long-wavelength fluctuations ($Q < 4 \times 10^{-3}$ Å) in materials that do not absorb visible light. The modulus of the scattering vector Q is defined by $Q = (4\pi/\lambda)\sin(\theta/2)$, where θ is the scattering angle and λ is the X-ray wavelength. The use of coherent X-rays for performing photon correlation spectroscopy enables the study of slow dynamics comparable to the timescales probed by DLS (10^{-3} to 10^7 Hz) on submicron, mesoscopic length scales ($10^{-3} < Q < 1$ Å^{-1}), thus enlarging the accessible Q range of DLS. In addition, this technique is not sensitive to multiple scattering (Grübel *et al.*, 2000; Robert *et al.*, 2005*a*), a problem usually occurring with DLS.

We present here experimental results that use the capabilities of two-dimensional (2D) XPCS to probe the dynamics at large wavevectors of optically opaque samples. We measure the self-diffusive properties (*i.e.* the asymptotic behavior of the effective diffusion coefficient for large wavevectors) of a colloidal dispersion.

2. Dynamics of a colloidal dispersion

2.1. Speckle patterns

When coherent light is illuminating a disordered system, such as a colloidal suspension, the instantaneous far-field scattering produces a random diffraction pattern or 'speckle pattern' (Grübel & Zontone, 2004) as illustrated in Fig. 1. These speckle patterns are related to the exact spatial arrangement of the scatterers, as a result of the interference of the scattered waves from all particles within the coherently illuminated volume.
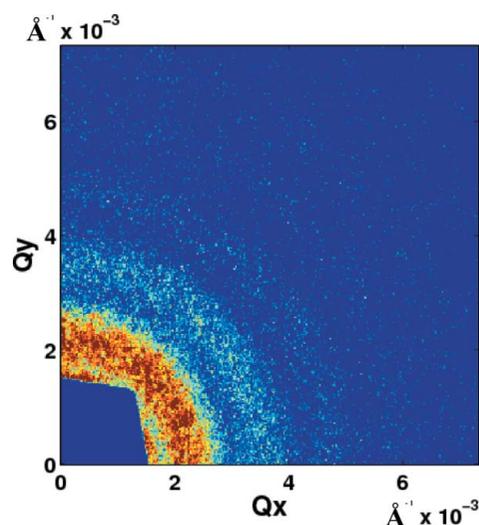

Figure 1
One of the measured 'time-resolved' 2D speckle patterns from the colloidal silica dispersion. The acquisition time was 1 s. The feature located close to (0, 0) is the shadow of the beamstop. An example of the time evolution of these patterns is available as supplementary material.[1]

If the spatial arrangement of the scatterers changes with time, as in the case of colloidal particles dispersed in a fluid phase, *i.e.* undergoing Brownian motion, one will observe that the corresponding speckle patterns also change and evolve with time, as shown on the movie presenting the time evolution of the recorded speckle patterns (available as supplementary material[1]). A characterization of the temporal intensity fluctuations $I(Q, t)$ at a given wavevector Q within the speckle pattern can thus reveal information on the underlying dynamics of the system.

2.2. Intensity autocorrelation function

In a classical photon correlation spectroscopy experiment (*i.e.* with a zero-dimensional detector) one places a detector with an aperture

---

‡ Present address: SLAC, Stanford University, USA.

[1] A time-resolved movie presenting the evolution of the speckle patterns is available from the IUCr electronic archives and can be viewed in the online version of this paper (Reference: CJ6012). Services for accessing these data are described at the back of the journal.

roughly equal to the size of a single speckle in the far-field scattering region of the sample. The registered signal, which is proportional to the fluctuating intensity $I(Q, t)$, is processed in a digital auto-correlator to produce the normalized intensity autocorrelation function $g^{(2)}(Q, \tau)$ defined as (Pusey, 1989)

$$g^{(2)}(Q, \tau) = \frac{\langle I(Q, t)I(Q, t + \tau)\rangle}{\langle I(Q, t)\rangle^2}, \tag{1}$$

where the angular brackets $\langle\ldots\rangle$ denote the ensemble average. For equilibrium dynamics, the time average is equivalent to the ensemble average, thus allowing the intensity autocorrelation function to be obtained with a point detector connected to a digital autocorrelator. The intensity autocorrelation function is connected to the normalized intermediate scattering function (ISF) $f(Q, \tau)$ via

$$g^{(2)}(Q, \tau) = 1 + \beta(Q)|f(Q, \tau)|^2, \tag{2}$$

where $\beta(Q)$ is the contrast and depends on the coherence properties of the beam and on the overall optical setup. For Brownian particles [i.e. a diluted dispersion of non-interacting particles, e.g. Grübel et al. (1999)], $f(Q, \tau)$ is expected to be in the short-time limit an exponential decay (Pusey, 1989),

$$f(Q, \tau) = \exp(-\Gamma\tau), \tag{3}$$

with a Q^2 dependence of the relaxation rate $\Gamma(Q)$,

$$\Gamma(Q) = D_0 Q^2. \tag{4}$$

The proportionality factor D_0 is the Stokes–Einstein diffusion constant,

$$D_0 = \frac{k_B T}{6\pi\eta R_H}. \tag{5}$$

D_0 depends on the Boltzmann constant k_B, the temperature T, the hydrodynamic radius of the particle R_H and the shear viscosity η of the suspending medium.

2.3. Self-diffusion properties of colloidal dispersions

For interacting colloidal systems, in the short-time limit the same formalism can be used, replacing the diffusion constant D_0 by a Q-dependent effective diffusion constant $D(Q)$. It presents deviations from D_0 that can be interpreted by the presence of two different interaction phenomena (Pusey, 1989).

The first one is related to the direct interactions in the system and is quantified by measuring the static structure factor $S(Q)$, which can be related to the mean-field interaction potential between the particles. It is classically measured with small-angle scattering techniques. The second one is related to many-body indirect interactions that are mediated by the solvent. This can be quantified by accessing the so-called hydrodynamic function $H(Q)$ [i.e. it is related to the coupling of the mobility tensor and requires a N-body approach for concentrated dispersions (cf. Beenakker & Mazur, 1984)].

The effective diffusion coefficient is connected to these two quantities by

$$D(Q) = \frac{D_0}{S(Q)}H(Q). \tag{6}$$

A slowing down of the diffusion around the peak in $S(Q)$ is expected and is often referred to as the cage effect. However, there is still an open question about the diffusion behavior in the small and large wavevector limits. In the limit of small wavevectors, $Q \to 0$, collective dynamics, characterized by a collective diffusion coefficient D_C, are probed. For large Q one expects to probe the individual dynamics, i.e.

the self-diffusive properties of the particles within the cage formed by the neighboring particles.

The asymptotic behavior of the effective diffusion coefficient $D(Q \to \infty)$ for large wavevectors is in fact a direct measure of a specific value of the hydrodynamic function, i.e. $H(\infty)$, and is referred to as the short-time self-diffusion coefficient D_S.

For large wavectors (i.e. typically for $QR > 5$), equation (6) simplifies to

$$D_S = D(Q \to \infty) = D_0 H(\infty), \tag{7}$$

as $S(Q \to \infty) = 1$ by definition (Pusey, 1989).

For hard-sphere systems, the volume-fraction dependence of the self-diffusion constant has been predicted (Beenakker & Mazur, 1984; Nägele et al., 1993) and experimentally measured (Segré et al., 1995). D_S is expected to be smaller than the Stokes–Einstein diffusion constant D_0 and to decrease with increasing volume fraction. The theoretical evaluation of $H(\infty)$ from Nägele et al. (1993) is expected to be identical for hard-sphere and charge-stabilized systems and is expressed to the second order in volume fraction Φ as

$$H(\infty) = (D_S/D_0) = 1 - 1.72\Phi + 0.88\Phi^2. \tag{8}$$

For very dilute samples (i.e. $\Phi \ll 1$) the self-diffusion coefficient D_S is expected to be identical to the Stokes–Einstein diffusion constant D_0.

3. Experimental details

The investigated sample consists of spherical colloidal silica particles dispersed in glycerol. These particles are slightly charge-stabilized. A highly turbid sample with volume fraction $\Phi = 0.1$ (as obtained from the measurement of the weight fraction of particles during the dispersion process) was placed in a thin quartz capillary.

The XPCS experiment was carried out at the ID10C branch of the Troïka beamline at the European Synchrotron Radiation Facility (ESRF) with X-rays of energy of 8 keV ($\lambda = 1.54$ Å) selected by a double-bounce Si(111) monochromator operating in horizontal scattering geometry. A collimated and partially coherent X-ray beam is obtained by using a pinhole with a diameter of 20 µm. The scattering intensity (speckle pattern) is recorded 3.3 m from the sample by a direct-illumination charge-coupled device (CCD) area detector (Princeton Instruments). As an illustration, a measured speckle pattern is presented in Fig. 1, with its typical and characteristic grainy appearance. The CCD pixel size is 20×20 µm. The sample is cooled down to $T = 259.55$ K. At this temperature the viscosity of the glycerol is $\eta = 56.193$ Pas.

A time series of speckle patterns was recorded (a sample 'speckle movie' is available as supplementary material) where one can clearly observe the speckle intensity fluctuations, especially at low Q where the dynamics are the slowest. The movie is made using measured data and with a speed of 50 times real time, in order to calculate the ensemble-averaged intensity autocorrelation using a multi-Q, multi-τ autocorrelator algorithm (Cipelletti & Weitz, 1999),

$$g^{(2)}(Q, \tau) = \frac{\langle I_{ij}(Q, t)I_{ij}(Q, t + \tau)\rangle_{ij}}{\langle I_{ij}(Q, t)\rangle_{ij}\langle I_{ij}(Q, t + \tau)\rangle_{ij}}, \tag{9}$$

where $\langle\ldots\rangle_{ij}$ denotes an average over a selection of intensities I_{ij} at pixels (i, j), defining a specific Q (which here corresponds to a circular average). The minimum lag time τ, set by the acquisition time of a single frame (1 s) and the transfer rate of the CCD (0.51 s), is 1.51 s. (Speckle patterns were acquired at this rate over about 3 h.) The correlation functions are obtained by performing circular averages at given values of Q, thus performing the required ensemble average.
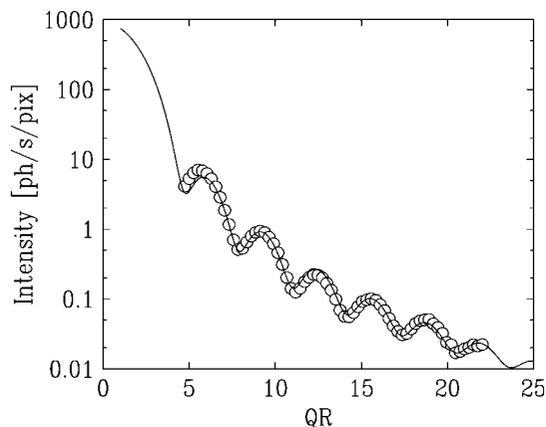
Figure 2
Small-angle X-ray scattering intensity obtained from the radial average of the mean of all the recorded speckle patterns. The solid line is the fit to the data, using a model describing the form factor for an assembly of polydisperse spheres with a Schultz size distribution function. The fitted radius and size polydispersity of the spheres are $R = 2608 \pm 5$ Å and $\delta = 0.03$, respectively.

The large number of pixels defining a single wavevector (*i.e.* typically larger than a thousand) allows high-quality data to be obtained even for weakly scattering samples. It also allows the dynamics of non-ergodic systems to be measured properly, as one would expect, for example, for probing the dynamics of glassy colloidal systems, where a proper ensemble average is required. This has recently been performed in two experiments (Robert *et al.*, 2006; Bandyopadhyay *et al.*, 2004). As an example, the ISF at $QR = 15.5$ displayed in Fig. 3 was obtained with a mean number of X-ray photons per pixel per second of 0.1 (*cf.* Fig. 2) and the number of pixels contained in the annulus defining $QR = 15.5$ was 4491. For comparison, the time required to access the same ISF with a comparable accuracy and a point detector (with identical spatial resolution, *i.e.* 20×20 μm) connected to a digital autocorrelator would be 562 days! In addition, 2D XPCS is probing the dynamics of the sample over the entire Q range simultaneously. This feature allows the dynamics of out-of-equilibrium systems to be probed and should open up new perspectives in this field (*cf.* Robert *et al.*, 2006; Bandyopadhyay *et al.*, 2004).
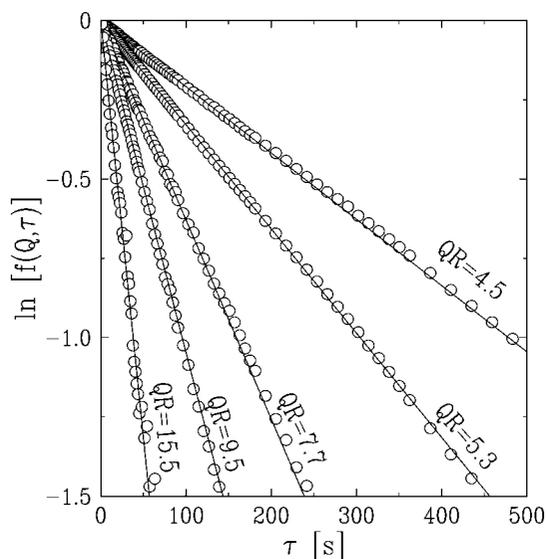
4. Experimental results

4.1. Small-angle X-ray scattering

We first characterized the colloidal dispersion by measuring its small-angle X-ray scattering (SAXS). This was obtained by circularly averaging the mean of the whole series of time-resolved speckle patterns recorded during the XPCS experiment (*i.e.* equivalent to measuring the SAXS with an incoherent X-ray beam). It is presented in Fig. 2. The solid line is the fit to the data using a model describing the form factor for an assembly of polydisperse spheres with a Schultz size distribution function (Kotlarchyk & Chen, 1983). We obtained the mean radius of the spheres to be $R = 2608 \pm 5$ Å and a poly-dispersity of $\delta = 0.03$. The extremely low polydispersity makes it a model system for comparison with colloidal hydrodynamic theories, which until now do not include size polydispersity. The data are presented for $QR \geq 4.5$, as the smaller wavevectors are contained below the shadow of the beamstop covering the area close to $(Q_x, Q_y) = (0, 0)$ to protected the CCD from the strong direct beam intensity. The scattering intensity $I(Q) = S(Q)F(Q)$ [where $S(Q)$ is the static structure factor and $F(Q)$ the form factor] thus reduces to the single-particle form factor $F(Q)$ as $S(Q) = 1$ for these large wavevectors (Pusey, 1989).

4.2. Two-dimensional X-ray photon correlation spectroscopy

The correlation functions $g^{(2)}(Q, \tau)$ were evaluated for the whole series of recorded speckle patterns, from which the ISFs were extracted. A selection of ISFs are presented in Fig. 3 with their corresponding fit (solid lines) to equation (3) for $QR = 4.5, 5.3, 7.7, 9.5$ and 15.5. The high quality of the data unambiguously shows that the ISFs are single exponential decays for the whole Q range, in agreement with Lumma *et al.* (2000), in which a charge-stabilized colloidal sample of comparable volume fraction was investigated.

Fig. 4 summarizes the results of the fitting procedure from all the obtained ISFs. It presents the dispersion relation of the relaxation rate Γ as a function of QR. The dotted line shows the expected behavior for a system consisting of the same colloidal spheres but that are not interacting (*i.e.* undergoing free Brownian motion). The dispersion relation is given by equation (4) with $D_0^{Th} = 1.29 \times 10^{-17}$ m² s⁻¹ using the mean radius from the SAXS measure-

Figure 3
Measured normalized ISFs for $QR = 4.5, 5.3, 7.7, 9.5$ and 15.5. The solid lines are the fit to the data with a single exponential decay [*cf.* equation (3)].
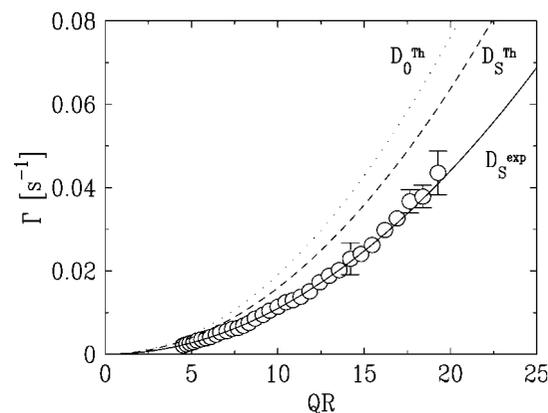

Figure 4
Dispersion relation (symbols) of the relaxation rate Γ. The dotted line is the prediction for the systems at infinite dilution (*i.e.* undergoing free Brownian motion) with the proportionality factor being the Stokes–Einstein diffusion constant $D_0^{Th} = 1.29 \times 10^{-17}$ m² s⁻¹. The solid line is a fit to the data assuming a Q^2 'parabolic' behavior. It gives the self-diffusion constant $D_S^{exp} = 7.5 \times 10^{-18}$ m² s⁻¹. The dashed line is the predicted dispersion using equation (8), giving $D_S^{Th} = 1.08 \times 10^{-17}$ m² s⁻¹.

ment as input to equation (5). As expected, the data strongly differ from free Brownian behavior. With the large QR range explored here [*i.e.* > 4.5, in contrast with Lumma *et al.* (2000) who investigated the dynamics in the vicinity the maximum of the static structure peak, *i.e.* $QR < 7$] one expects the experiment to be only sensitive to the self-diffusion constant D_S. This is perfectly in agreement with theory as the experimental observations present a 'parabolic' Q^2 dependence of the relaxation rate.

The result of the fit to equation (4), displayed by the solid line in Fig. 4, replacing D_0 by D_S^{exp}, gives the measured self-diffusion constant $D_S^{exp} = 7.5 \times 10^{-18}$ m^2 s^{-1} and $H^{exp}(\infty) = D_S^{exp}/D_0 = 0.579$. It contrasts strongly with previous measurements by Lumma *et al.*, where the dynamics were 'showing quantitative agreement' with a hard-sphere theoretical model. Our result is here in contradiction with the theoretical prediction given by equation (8) [*i.e.* $H^{Th}(\infty) = 0.837$], giving $D_S^{Th} = 1.08 \times 10^{-17}$ m^2 s^{-1} as shown by the dashed line in Fig. 4.

The experimental value $H^{exp}(\infty) = 0.579$ is observed to be smaller than the theoretical one. This points towards a lack of colloidal hydrodynamic theories (Beenakker & Mazur, 1984; Nägele *et al.*, 1993), in which the hydrodynamic behavior is assumed to be identical for hard-sphere and charge-stabilized systems.

Until now experimental confirmation of equation (8) has been obtained on hard-sphere systems only (*e.g.* Segré *et al.*, 1995). However, the system investigated here is known to be weakly charge-stabilized. This could be the origin of the observed discrepancy between $H^{exp}(\infty)$ and $H^{Th}(\infty)$. Recent measurements (Grübel *et al.*, 2000; Robert, 2001; Robert *et al.*, 2005b) of the whole Q dependence of the hydrodynamic function $H(Q)$ for charge-stabilized colloidal dispersions in non-dilute solutions (*i.e.* $\Phi > 0.04$) have shown similar behavior and tend toward the same conclusion. The charge-stabilized system investigated by Lumma *et al.* is, however, described 'quantitatively' by the hard-sphere model from the static, dynamic and hydrodynamic points of view, and points towards a small contribution of the electrostatic direct interactions.

5. Conclusion

We used 2D XPCS to probe the dynamics of an opaque colloidal dispersion. The large wavevector behavior, *i.e.* where the static structure factor $S(Q) = 1$, was probed. We mapped out the Q dependence of the normalized ISFs. The high 2D XPCS data quality, resulting from the ensemble average for each wavevector over a large number of pixels from the 2D speckle patterns, allowed the data to be unambiguously modeled with single exponential decays using equation (3).

The dispersion relation of the relaxation rate Γ is observed to have a 'parabolic' Q^2 dependence, thus confirming that the self-diffusive properties can be modeled with equation (4), just replacing the Stokes–Einstein diffusion constant D_0 by the self-diffusion constant D_S^{exp}.

The measured self-diffusion constant D_S^{exp} is observed to be smaller than the theoretical one, D_S^{Th}. We do thus observe slower dynamics than expected, which points towards a lack of modeling for colloidal many-body hydrodynamic theories, which until now assume that the hydrodynamic behavior is identical for charge-stabilized and hard-sphere particles.

These results, in combination with recent measurements of the complete Q dependence of the hydrodynamic function $H(Q)$, clearly demonstrate that the charge-stabilized character of the particles should be taken into account.

From a phenomenological point of view the presence of the surface charges, resulting in a screened Coulomb interaction potential, slows down the dynamics of the system as compared to dispersion of non-charged particles of identical volume fraction.

References

Bandyopadhyay, R., Liang, D., Yardimci, H., Sessoms, D. A., Borthwick, M. A., Mochrie, S. G. J., Harden, J. L. & Leheny, R. L. (2004). *Phys. Rev. Lett.* **93**, 228302(1–4).
Beenakker, C. J. W. & Mazur, P. (1984). *Physica A*, **126**, 349–370.
Cipelletti, L. & Weitz, D. A. (1999). *Rev. Sci. Instrum.* **70**, 3214–3221.
Grübel, G., Abernathy, D. L., Riese, D. O., Vos, W. L. & Wegdam, G. W. (2000). *J. Appl. Cryst.* **33**, 424–427.
Grübel, G., Robert, A. & Abernathy, D. L. (1999). *Slow Dynamics in Complex Systems*, Eighth Tohwa University International Symposium, edited by M. Tokuyama and I. Oppenheim, pp. 158–159.
Grübel, G. & Zontone, F. (2004). *J. Alloys Comput.* **362**, 3–11.
Kotlarchyk, M. & Chen, S. H. (1983). *J. Chem. Phys.* **79**, 2461–2469.
Lumma, D., Lurio, L. B., Borthwick, M. A., Falus, P. & Mochrie, S. G. J. (2000). *Phys. Rev. E*, **62**, 8258–8269.
Nägele, G., Kellerbauer, O., Krause, R. & Klein, R. (1993). *Phys. Rev. E*, **47**, 2562–2574.
Pusey, P. (1989). *Les Houches: Liquids, Freezing and Glass Transition*, edited by J. P. Hansen, D. Lesveque & J. Zinn-Justin, pp. 763–941. Amsterdam: Elsevier.
Robert, A. (2001). PhD Thesis, Univeristy of Grenoble, France.
Robert, A., Wagner, J., Autenrieth, T., Härtl, W. & Grübel, G. (2005a). *J. Magn. Magn. Mater.* **289**, 47–49.
Robert, A., Wagner, J., Autenrieth, T., Härtl, W. & Grübel, G. (2005b). *J. Chem. Phys.* **122**, 084701(1–6).
Robert, A., Wandersman, E., Dubois, E., Dupuis, V. & Perzynski, R. (2006). *Europhys. Lett.* **75**, 764–770.
Segré, P. N., Behrend, O. P. & Pusey, P. (1995). *Phys. Rev. E*, **52**, 5070–5083.